



OPEN

SUBJECT AREAS:

NANOPHOTONICS AND PLASMONICS

TERAHERTZ OPTICS
METAMATERIALSReceived
12 August 2013Accepted
13 September 2013Published
8 October 2013

Correspondence and requests for materials should be addressed to J.H.T. (jh-teng@imre.a-star.edu.sg)

Nano-antenna in a photoconductive photomixer for highly efficient continuous wave terahertz emission

H. Tanoto¹, J. H. Teng¹, Q. Y. Wu¹, M. Sun², Z. N. Chen^{2,3}, S. A. Maier⁴, B. Wang¹, C. C. Chum¹, G. Y. Si³, A. J. Danner³ & S. J. Chua³¹Institute of Materials Research and Engineering, Agency for Science, Technology and Research (A*STAR), Singapore 117602,²Institute for Infocomm Research, Agency for Science, Technology and Research (A*STAR), Singapore 138642, ³Department of Electrical and Computer Engineering, National University of Singapore, Singapore 117576, ⁴Department of Physics, Imperial College London, London SW7 2AZ, UK.

We report highly efficient continuous-wave terahertz (THz) photoconductive antenna based photomixer employing nano-gap electrodes in the active region. The tip-to-tip nano-gap electrode structure provides strong THz field enhancement and acts as a nano-antenna to radiate the THz wave generated in the active region of the photomixer. In addition, it provides good impedance matching to the THz planar antenna and exhibits a lower RC time constant, allowing more efficient radiation especially at the higher part of the THz spectrum. As a result, the output intensity of the photomixer with the new nano-gap electrode structure in the active region is two orders of magnitude higher than that of a photomixer with typical interdigitated electrodes. Significant improvement in the THz emission bandwidth was also observed. An efficient continuous wave THz source will greatly benefit compact THz system development for high resolution THz spectroscopy and imaging applications.

The terahertz (THz) electromagnetic waves have unique properties such as low photon energy, finger-print spectral range for biomolecules, and transparency to some optically-opaque materials, such as clothing and papers, and have already found far-reaching applications ranging from molecular spectroscopy, to astronomy, environmental monitoring, bio-imaging, security screening and many others^{1–6}. One of the most critical challenges in the development of terahertz systems is the lack of compact efficient room-temperature sources, especially tunable continuous-wave sources with narrow bandwidth for high resolution spectroscopy and imaging^{5,6}. Semiconductor based sources are promising to be compact, economical and highly efficient. Quantum cascade lasers (QCLs) are one promising candidate of CW THz sources^{7–10}, however, for operation especially at the lower THz range, a cryogenic cooling is still required. The highest reported operating temperature without external magnetic field was 186 K at 3.9 THz and 163 K at 1.8 THz^{11,12}. Major efforts are currently underway to further increase the operating temperature and lowering the operating frequency. A promising technique for realizing room temperature CW THz sources is the photomixing in ultrafast photoconductive semiconductor materials^{13–16}, the photomixer also performs best at low THz frequency and with high-resolution tunability. The efficiency of photomixers is determined by the internal efficiency of the semiconductor materials employed and the efficiency of the metal planar antenna in radiating the THz waves. Currently, the low efficiency of both parts limits the output power of CW THz photomixers¹⁷.

Optimizations of photomixer materials and designing efficient THz antennas^{18–23} have been the major focus of research in this area for the past decade. On the other hand, there was less focus on improving the efficiency of the active region of the photomixer, where optical pump is subjected to and which is the current source in the photomixer equivalent circuit. Interdigitated electrode structures, originally used in metal-semiconductor-metal (MSM) photodetectors²³, have been widely used in the active region to improve the efficiency of photon to current conversion. However, optimization of the interdigitated electrode structures leads to trade-off between electrode finger separation and photocarrier generation intensity. In order to achieve higher efficiency, the transit time for photogenerated carriers should be reduced, which requires reduction in the finger electrode separation. Such a strategy leads to a smaller photoconductive area being exposed to the impinging optical pump laser, and hence lesser photogenerated carriers. A new active region structure design that can circumvent this limitation is desired in order to significantly improve the efficiency of CW THz photomixer.

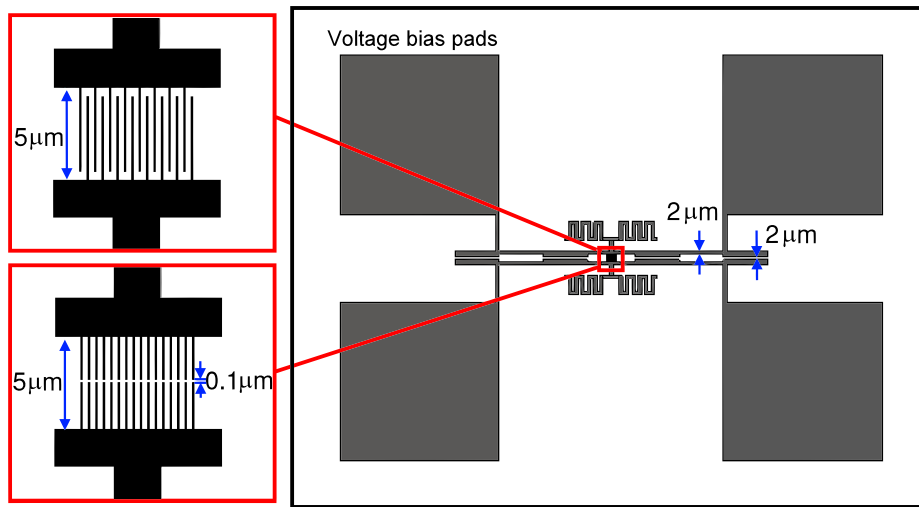


Figure 1 | Schematic drawings of the fabricated CW THz photomixers. The enclosed schematic on the right shows the overall antenna structure with four bias pads and a modified Meander THz antenna design. The two enclosed drawings on the left show the active region designs with interdigitated electrodes shown at the top and tip-to-tip nano-gap electrodes shown at the bottom.

Plasmonic metamaterials provide unique opportunities in manipulating electromagnetic waves in the THz range. Many novel THz devices have been demonstrated, such as THz guiding by spoof surface plasmon polaritons^{24–26}, frequency agile filters and modulators^{27,28}, perfect absorber²⁹ and collimation of a THz QCL beam³⁰. It was also reported that the THz field can be enhanced by orders of magnitude in a metal nano-slit (70 nm) far-beyond the skin-depth³¹. And recently, plasmonic electrode structures were used to demonstrate significant enhancement in pulsed THz photoconductive emitter used in femtosecond laser based THz time domain system³². However, implementation of plasmonic metamaterials to enhance the performance of the most critical and desired CW THz sources has yet been demonstrated. In this paper, we report nano-gap electrodes as the active region in a photoconductive antenna (PCA) based CW THz sources to enhance the localized field of both the near-infrared light and the THz wave. We demonstrate two-orders of magnitude enhancement in THz emission intensity compared to a conventional photomixer using interdigitated electrodes.

Results

The investigated devices consist of 1 μm thick low-temperature grown GaAs and 1 μm thick AlAs heat-spreading layer grown on a semi-insulating GaAs substrate using solid-source molecular beam epitaxy (MBE). The low-temperature grown GaAs (LT GaAs) has been shown to feature high-resistivity, high carrier mobility and ultra-short carrier lifetime, suited for photomixing^{14–18}. The details of semiconductor materials properties and fabrication are presented in the Methods section. Schematic drawings with dimensions of the devices are presented in Fig. 1. The width and separation of the electrode fingers of the active region are 100 nm and 300 nm respectively, the same for both interdigitated and tip-to-tip nano-gap electrodes. Plan-view scanning electron microscope (SEM) images of the photomixer with interdigitated electrodes and tip-to-tip nano-gap electrodes are presented in Fig. 2. Both devices employed a modified Meander antenna that has similar effective radiating parts as a simple dipole antenna but with a better impedance matching.

The devices were tested at the same DC bias voltage of 15 V and excited by two tunable distributed feedback (DFB) lasers. The tunable lasers had central emission wavelengths of 852 nm and 855 nm, respectively, with a total output power of 90 mW after optical amplifier. The THz wave emitted from the GaAs substrate backside was coupled to a silicon hyper-hemispherical lens and measured by

vacuum Fourier-transform infrared spectroscopy (FTIR) with a liquid helium-cooled silicon bolometer detector. A schematic of the measurement setup is shown in Fig. 3.

Selected emission spectra of the tip-to-tip nano-gap photomixer as recorded by the FTIR system are shown in Fig. 4a. The x-axis is the wave number, with 33.33 cm^{-1} approximately equal to 1 THz in frequency. Tip-to-tip nano-gap photomixer emission spectra from 7 cm^{-1} to 33 cm^{-1} are presented in the plot. The actual recorded emissions are up to 53 cm^{-1} , but are not presented due to the large intensity difference with the spectrum below 33 cm^{-1} . The inset of Fig. 4a shows the emission spectra of the interdigitated photomixer; the emission spectra have similar shape to that of the tip-to-tip nano-gap photomixer, but with much lower intensity. The peak position of the THz emission in Fig. 4a is equal to the laser offset. As an example, for peak position of 11.7 cm^{-1} , the laser offset frequency would be 0.35 THz. The very narrow linewidth characteristic of a CW THz

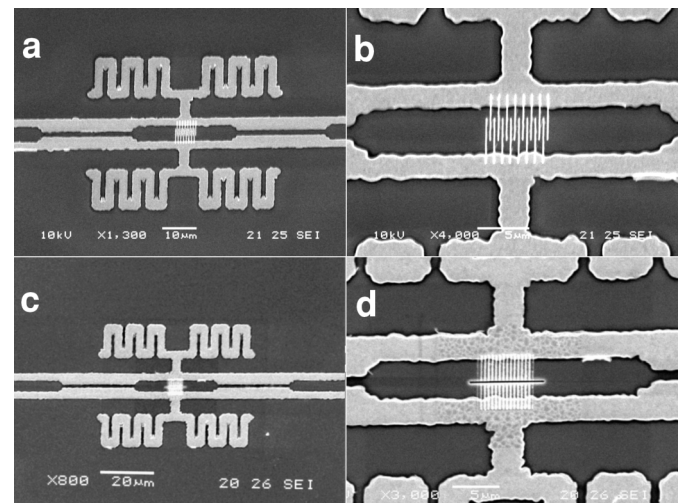


Figure 2 | Plan-view SEM images of the CW THz photomixers.

(a), Overall antenna structure, the modified Meander THz antenna is apparent here. (b), A zoom-in view of interdigitated electrodes at the active region. (c), Overall antenna structure of the device with the new active region design. (d), A zoom-in view of tip-to-tip nano-gap electrodes at the active region, the gap of 100 nm at the centre was defined by a focused ion beam (FIB) milling.

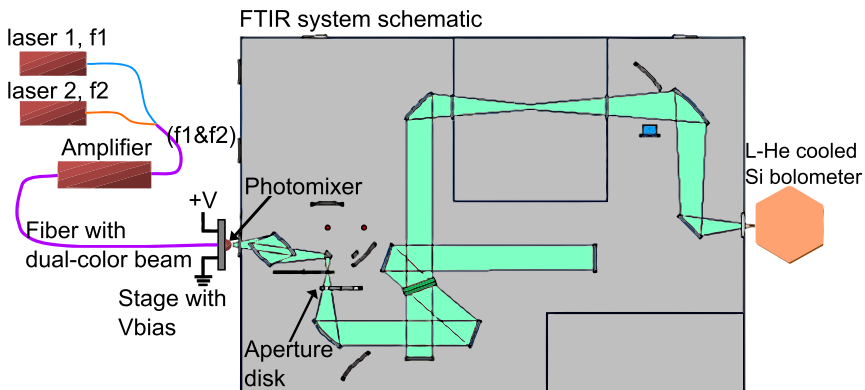


Figure 3 | A schematic drawing of the photomixers testing setup. The liquid-He cooled Si bolometer used to detect the emitted THz wave is attached to a Bruker 80v vacuum FTIR system.

photomixer emission, which is determined by the linewidth of the pump lasers, < 10 MHz in our case, is promising for high resolution spectroscopy. The recorded emission spectra linewidth is limited by the resolution of the FTIR system of ~ 6 GHz.

Significant enhancement in the emission intensity is observed across a bandwidth of ~ 1.3 THz for the tip-to-tip nano-gap electrode photomixer as compared to the interdigitated photomixer, as

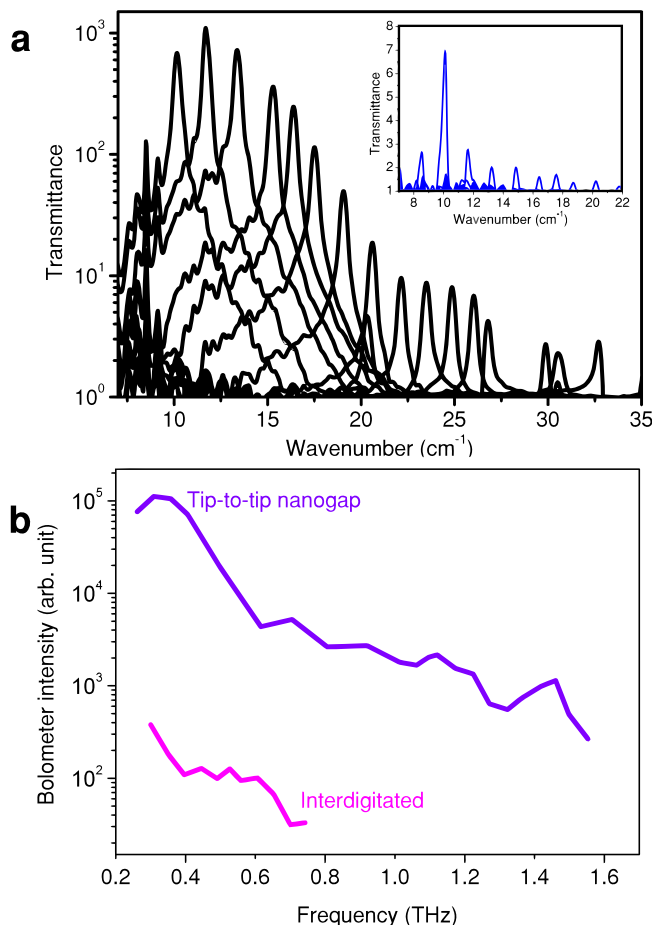


Figure 4 | Terahertz output characteristics of the photomixers.

(a), Emission spectra of the tip-to-tip nano-gap photomixer as recorded at different laser offset frequency. Inset: emission spectra of the interdigitated photomixer, note the much lower intensity compared to the tip-to-tip nano-gap photomixer. (b), Output intensity comparisons between the CW THz photomixer with interdigitated electrodes and tip-to-tip nano-gap electrodes.

shown in Fig. 4b. The level of enhancement of the output intensity is approximately two orders of magnitude across the range. At around 400 GHz, the enhancement from the nano-gap photomixer is more than three orders of magnitude. These measurement results clearly demonstrate the advantages of using planar THz antennas coupled with tip-to-tip nano-gap active region, leading to highly efficient CW THz photomixers. To understand the origin of the enhancements, we performed electromagnetic field simulations employing CST Microwave Studio and finite difference time domain (FDTD) simulation software.

Discussion

When two optical electromagnetic waves with frequency f_1 and f_2 are subjected onto the photomixer, the materials and the antenna can respond only to the lower envelope frequency, which is $|f_1 - f_2|$. An AC current with frequency of $|f_1 - f_2|$ is induced by the movements of photogenerated carriers between the DC biased planar metal electrodes on the photomixer materials. The E-field distribution in the near-field of the entire structure including the active photomixing region and the Meander antenna under illumination by a 1 THz plane wave was simulated using CST Microwave Studio. Localized sub-meshing was used in the photomixer active region or the illuminated electrodes area to enhance the accuracy. The metal electrodes and planar antenna were modelled as perfect electrical conductors (PEC). The results for the tip-to-tip nano-gap electrodes photomixer and the conventional interdigitated electrodes photomixer are shown in Figs. 5a and 5b respectively. The dimensions used in the simulations were the same as the ones presented in Fig. 1.

The E-field (E_0) of the incident THz plane wave was kept at 1 V/m for both structures. From Fig. 5a, it can be seen clearly that the electric field intensity is greatly enhanced within the tip-to-tip nano-gap region predominantly due to a nano-antenna effect, similar to the well-known lightning rod effects³³. For this structure, the E-field of incident THz plane wave was aligned along the y -axis, in accordance with the direction of the electric field under DC bias. The lightning-rod-assisted evanescent tunnelling through the sub-wavelength gap allows the incident THz wave arriving on the metal electrode surface to be transmitted more intensely. The active region in this case not only acts as current source, but also contributes to the overall emission of THz waves, behaving as nano-antenna. Due to the intense E-field at the active region, which is analogue to a current source, the E-field intensity radiated at both arms of the dipole antenna structure is also enhanced.

As for the structure in Fig. 5b, the E-field of the incident THz plane wave was chosen to be polarized along the x -axis so as to make it parallel with the dominant direction of electric field during DC biased. The structure exhibits much lower E-field amplitude. Due to the fact that the interdigitated electrode configuration resembles

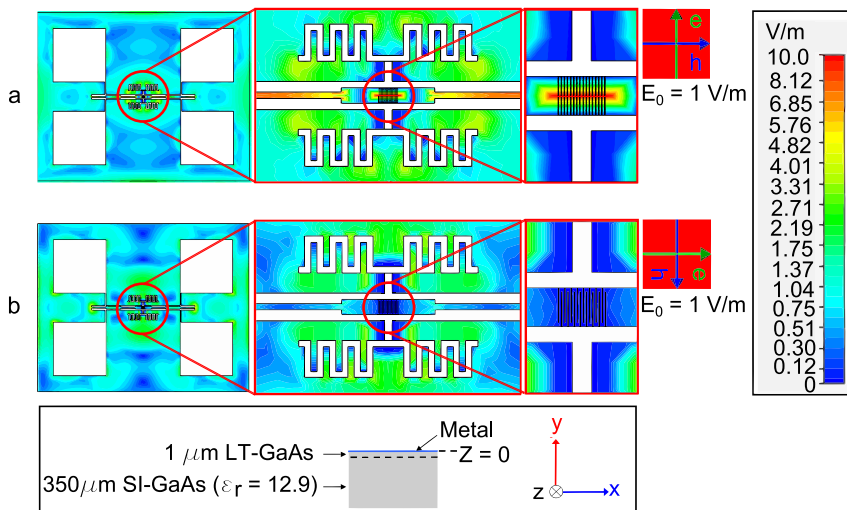


Figure 5 | Amplitude of electric field in the near-field of a modified Meander antenna with different photomixers at 1 THz plane-wave illumination. (a), A photomixer with the tip-to-tip nano-gap electrodes. (b), A photomixer with typical interdigitated electrodes. (inset) A cross section schematic of the devices and the axis convention used in the simulation.

parallel plate capacitors, the electromagnetic energy is being stored rather than being emitted out. Therefore, although enhancement is also present in this configuration, the E-field was not radiated but trapped in the substrate instead. Measured polarization of the THz wave emitted from both types of photomixer showed that the nano-gap electrode photomixer indeed showed much stronger vertical (y -axis) polarization than the interdigitated one in the lower THz range where the resonance occurred.

With the two-color optical inputs containing a beat signal oscillating in the THz regime and as the width of the electrodes is much smaller than the wavelength, strong electric field localization and confinement should occur for the THz wave^{31,34–37}. We employed FDTD simulations to find out the field enhancement factor. Again, a plane wave at wavelength of 300 μm (1 THz) was used to illuminate the structure. The dimensions of the device are presented in Fig. 1 with the gap of the tip-to-tip nano electrodes as the only variable. Figure 6a shows the field intensity enhancements as compared to the interdigitated structure as the gap in the tip-to-tip nano-gap electrode structures was varied from 50 nm to 1000 nm. The field intensity is obtained at the center of the gap. It was found that the enhancement can be as large as 400 times in a 50 nm gap and 100 times in a 100 nm wide gap, the same dimension used in the test devices. The results are in agreement with those reported by M. A. Seo *et al.*³¹. As a comparison, we also calculated the field enhancement factor at the 850 nm pumping light, the enhancement can be observed only when the gap is < 100 nm. Figures 6b and 6c show the electric field intensity distributions in the tip-to-tip nano-gap electrode structures for a 50 nm gap and 1000 nm gap, respectively. With the electric-field component of the incident electromagnetic waves aligned in the y -direction, as the gap between two opposing electrodes narrows down, the charge at the tip of opposing electrodes experience stronger attraction, subsequently inducing greater accumulation of charges. The enhanced surface charge accumulations are the origin of the field enhancement shown in Fig. 6a. On the other hand, as the opposing electrodes are moved further apart, the attraction between surface charges becomes weaker, and at 1000 nm apart there is no enhancement within the gap and the field is only concentrated at the tip of electrodes, as shown in Fig. 6c.

In the case of the interdigitated electrodes structure, the field is also enhanced due to surface charge interaction. However, the strength of the enhancement is restricted by the width of the electrodes. This is because the surface charge density is limited by the total charge

number per unit width of the electrode fingers as the electric field of the incident electromagnetic waves is aligned perpendicularly to the electrode fingers. Therefore, the surface charges density is not as large as in the case of tip-to-tip nano-gap electrodes with the electric field aligned along the electrodes fingers length. Due to the electrode width limiting the surface charges, even if the separation between two electrode fingers is made smaller, there will not be field enhancement as significant as in the case of tip-to-tip nano-gap electrodes configuration. Furthermore, due to the broken symmetry in the y -axis of the interdigitated electrodes, part of the electric field component would deviate along this axis and induces charge flow along the electrode fingers length. These charges finally accumulate at the electrodes tips. The charges accumulation at the electrodes side surfaces in stronger field compared to field on the electrodes side surfaces.

The electric field distribution underneath the electrodes during DC bias in both devices differs significantly due to the structural and configuration aspects. In the case of the CW THz photomixer with tip-to-tip nano-gap electrodes, the E-field intensity within the gap was enhanced by at least three times due to the proportionally smaller gap between opposing electrodes compared to the device with typical interdigitated electrodes, which is 100 nm vs. 300 nm, respectively. The edge effects affect the distributions of the electric field as well with significant increment of charge collection ability at the edge of electrodes. This improves the near-anode photogenerated carriers capture mechanism by the electrodes, which increase both the DC and THz photocurrent.

We have also investigated the effect of the meander antenna structures to the characteristics of the photomixers. For both tip-to-tip nano-gap and interdigitated electrodes, the active region can be regarded as a capacitor-like THz current source. It can be modeled by a discrete current source in CST Microwave Studio to excite the meander antenna. The region between the electrodes and bias pads has the chock acting as a filter to minimize the flow of RF currents into the bias lines to avoid unwanted radiation. The meander structure act as an inductive loading of the dipole to compensate the capacitor-like active source for better impedance matching, and shifts the resonance frequency down to ~ 0.5 THz. The electrodes in the active region further enlarge the effective dipole length and have similar effects in shifting the antenna resonant frequency down to ~ 0.4 THz for tip-to-tip nano-gap electrodes, as can be observed in Fig. 4b. In the case of interdigitated electrodes, owing to the longer electrodes, the resonant frequency shifted even lower. This lower

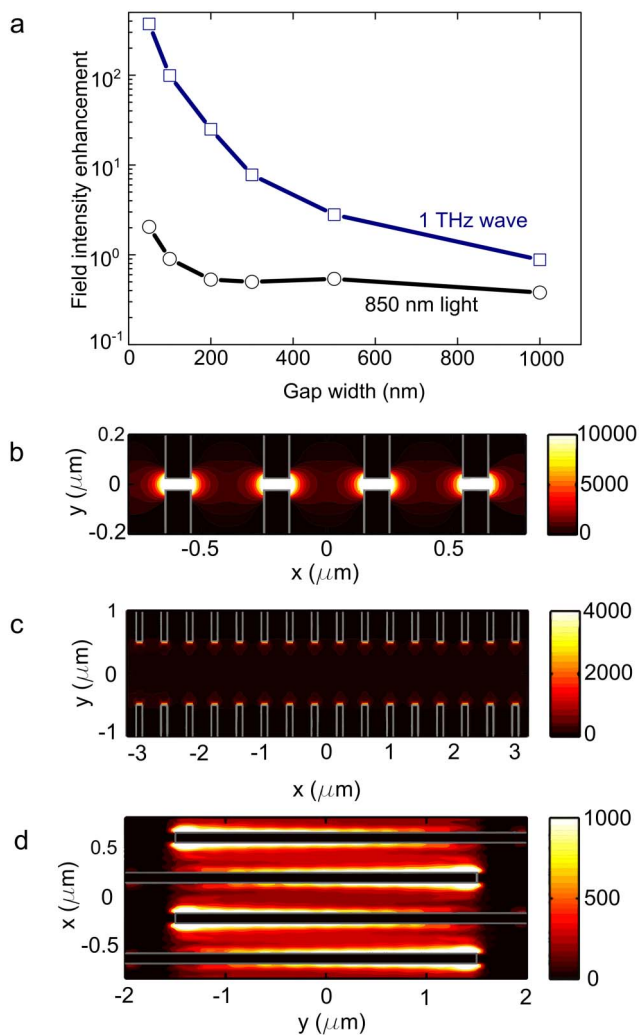


Figure 6 | The FDTD simulation of electric field enhancement as function of gap width and simulation of field intensity distributions within the active region under 1 THz plane wave illumination. (a), The electric field enhancement between the tip-to-tip nano-gap electrode structures with varying gap width and the typical interdigitated electrode structures. (b), The electric field intensity distribution for tip-to-tip nano-gap electrodes with 50 nm gap. The field intensity is greatly enhanced and concentrated within the gap. (c), The electric field intensity distribution for tip-to-tip nano-gap electrodes with 1000 nm gap is concentrated at the tips of the electrodes. (d), The electric field intensity distribution for interdigitated electrode configuration. The field at the tip of the electrodes is more intense compared to the field at the side surfaces of the electrodes.

resonant frequency leads to smaller efficiency at higher THz frequency for the photomixer with interdigitated electrodes, contributing to its smaller bandwidth as compared to the photomixer with tip-to-tip nanogap electrodes. Furthermore, the simulation confirms that the tip-to-tip nano-gap electrode has a much smaller capacitance than interdigitated electrodes while having a better impedance matching to the meander antenna. When we consider the equivalent circuit of a THz photomixer where it is simplified as capacitance and resistance, the relationship between the THz output power and the circuit capacitance is¹⁸

$$P_{THz}(\omega) \propto \frac{1}{1 + (\omega R_A C)^2} \quad (1)$$

where P_{THz} is the mean power of THz output, ω is the frequency, R_A is the antenna resistance and C is the capacitance of the photomixer.

Using COMSOL, we calculated the capacitance of the nano-gap electrode antenna structure to be 2.1 fF while the interdigitated one was found to be 3.2 fF. This translates to at least a factor of 2.3 enhancement of P_{THz} . A lower RC time constant also allows for better output intensity performance especially at the higher part of the THz spectrum.

In summary, a highly efficient CW THz source by employing nano-electrodes in the active region of the photomixer is demonstrated. Full-field electromagnetic simulations reveal that the photomixer active region with tip-to-tip nano-gap electrodes actively radiates THz waves, in contrast to the active region with typical interdigitated electrodes. FDTD simulations show two orders of magnitude field enhancements in the THz region in the tip-to-tip nano-gap electrodes with a 100 nm gap, compared to the interdigitated electrodes configuration. With the E-field of the impinging electromagnetic waves polarized parallel to the opposing electrodes, the enhanced THz field leads to a stronger force driving the photo-generated carriers to the electrodes more efficiently. The new active region structure also provides good impedance matching to the THz planar antenna and exhibits lower RC time constant allowing more efficient radiation especially at higher part of the THz spectrum. Measurement results from the fabricated photomixers show about two orders of magnitude output intensity enhancement and larger bandwidth in CW THz photomixer with the tip-to-tip nano-gap active region than that with conventional interdigitated electrodes.

The results presented here were previously published in *Nature Photonics*, 6, 121–126 (2012)³⁸. The paper was subsequently retracted after an error was found in the calculations for estimating the power output of the photomixers using blackbody power estimation. This estimation has been discarded in the current paper and instead we compare the output intensity of the photomixers as detected by the bolometer.

Methods

The investigated devices consist of 1 μm of low temperature grown GaAs (LT GaAs) and 1 μm of AlAs heat-spreading layer grown on a semi-insulating GaAs substrate using solid-source molecular beam epitaxy (MBE). The growth temperature for LT GaAs is ~300°C with *in-situ* post-growth annealing at 600°C for 10 minutes. Hall Effect measurements revealed a resistivity of ~5 × 10⁷ Ohm.cm and room temperature carrier mobility of ~5000 cm²/V.s. The carrier lifetime of the LT GaAs was found to be <1 ps, due to the effects of arsenic precipitates.

A modified meander antenna was adopted for the CW THz photomixer. The meander antenna was patterned using a standard photolithography and metal lift-off process. The LT-GaAs wafer was firstly cleaned with Acetone and Methanol for 5 minutes each and rinsed with DI wafer. The wafer was then baked in oven at 120°C for 10 minutes for dehydration. This was followed by AZ5214 photo-resist coating with spin speed 5000 rpm and soft bake at 90°C for 90 seconds. The photolithography was done by using mask aligner SUSS MicroTec (MA8/BA6). Ti/Au of 10 nm/150 nm was deposited using Denton Explorer electron beam evaporator and ultrasonic assisted liftoff to form the photoconductive antenna. To define the sub-micron electrodes, the patterned wafers were coated with PMMA with spin speed 3000 rpm. Soft bake was done at 180°C for 10 minutes. The interdigitated electrodes pattern and the nano-gap electrode pattern without the opening of the central gap were formed by electron beam lithography on PMMA using Elionix ELS-7000 EBL system at current of 100 pA and dose time 2.4 μsec/dot. The patterns were developed using MIBK:IPA (1:3). Ti/Au of 5 nm/100 nm was deposited by ebeam evaporation and liftoff process. A 100 nm nano-gap between the connected electrodes was defined by focused ion beam (FIB) milling using a FEI/FIB 200XP Single Beam FIB at 70 pA current.

The wafers were then diced and mounted on a hyper-hemispherical lens made of high-resistivity silicon from Batop GmbH. The electrode active region, also the pumping light illumination area has an area of approximately 5 μm × 8 μm. Voltage biasing of the device was achieved using probes attached to a Keithley source meter, which also function as photocurrent meter. Two tunable CW single frequency semiconductor lasers (Toptica DFB) operating at central wavelength of 852 nm and 855 nm were used as the excitation light source. The two laser beams were combined using a 2 × 1 single-mode polarization maintaining fiber. After amplification at the Toptica BoosTA semiconductor amplifier, the fiber-coupled combined laser beam was aligned to the photomixer active region using a Newport XYZ micrometer precision stage. The tuning of the laser frequency offset was done by carefully setting the two laser temperatures at calibrated temperature. At each frequency offset point, the emission spectra from the photomixer was obtained using FTIR in conjunction with L-He cooled Si bolometer. The characteristic of the emission of a photomixer is its narrow line width, as determined by the laser pump source. In our case, the laser



line width is <10 MHz. Nonetheless, the recorded emission spectra line width is limited by the resolution of the FTIR system of ~ 6 GHz.

Each of the photomixer was mounted on a dedicated stage with bias probes and placed directly in front of the FTIR input window. For data collection, we set the FTIR scanning range from 5 to 70 cm $^{-1}$ where 1 THz ~ 33.33 cm $^{-1}$. Acquisition mode used was single sided forward-backward, with scanning resolution 0.2 cm $^{-1}$. The Mylar 50 micron beam splitter was employed.

1. Winnewisser, G. Spectroscopy in the terahertz region. *Vibrat. Spectrosc.* **8**, 241–253 (1995).
2. Siegel, P. H. Terahertz technology. *IEEE Trans. Microw. Theory Tech.* **50**, 910–928 (2002).
3. Hu, B. B. & Nuss, M. C. Imaging with terahertz waves. *Opt. Lett.* **20**, 1716–1718 (1995).
4. Shen, Y. C. *et al.* Detection and identification of explosives using terahertz pulsed spectroscopic imaging. *Appl. Phys. Lett.* **86**, 241116 (2005).
5. Tonouchi, M. Cutting-edge terahertz technology. *Nature Photon.* **1**, 97–105 (2007).
6. Williams, B. S. Terahertz quantum-cascade lasers. *Nature Photon.* **1**, 517–525 (2007).
7. Qin, Q., Williams, B. S., Kumar, S., Hu, Q. & Reno, J. L. Tuning a terahertz wire laser. *Nature Photon.* **3**, 732–737 (2009).
8. Amanti, M. I., Fischer, M., Scalari, G., Beck, M. & Faist, J. Low-divergence single-mode terahertz quantum cascade laser. *Nature Photon.* **3**, 586–590 (2009).
9. Kumar, S., Chan, C. W. I., Hu, Q. & Reno, J. L. A 1.8-THz quantum cascade laser operating significantly above the temperature of $\hbar\omega/k_B$. *Nature Phys.* **7**, 166–171 (2011).
10. Maineult, W. *et al.* Metal-metal terahertz quantum cascade laser with micro-transverse-electromagnetic-horn antenna. *Appl. Phys. Lett.* **93**, 183508 (2008).
11. Kumar, S., Hu, Q. & Reno, J. L. 186 K operation of terahertz quantum-cascade lasers based on a diagonal design. *Appl. Phys. Lett.* **94**, 131105 (2009).
12. Ferguson, B. & Zhang, X. C. Materials for terahertz science and technology. *Nature Mater.* **1**, 26–33 (2002).
13. Preu, S., Döhler, G. H., Malzer, S., Wang, L. J. & Gossard, A. C. Tunable, continuous-wave Terahertz photomixer sources and applications. *J. Appl. Phys.* **109**, 061301 (2011).
14. McIntosh, K. A. *et al.* Terahertz photomixing with diode lasers in low-temperature-grown GaAs. *Appl. Phys. Lett.* **67**, 3844–3846 (1995).
15. Gregory, I. S. *et al.* Resonant dipole antennas for continuous-wave terahertz photomixers. *Appl. Phys. Lett.* **85**, 1622–1624 (2004).
16. Brown, E. R., McIntosh, K. A., Nichols, K. B. & Dennis, C. L. Photomixing up to 3.8 THz in low-temperature-grown GaAs. *Appl. Phys. Lett.* **66**, 285–287 (1995).
17. Brown, E. R. THz generation by photomixing in ultrafast photoconductors. *Int. J. High Speed Electron. Syst.* **13**, 497–545 (2003).
18. Gregory, I. S. *et al.* Optimization of photomixers and antennas for continuous-wave terahertz emission. *IEEE J. Quant. Electron.* **41**, 717–728 (2005).
19. Duffy, S. M. *et al.* Accurate modeling of dual dipole and slot elements used with photomixers for coherent terahertz output power. *IEEE Trans. Microw. Theory Tech.* **49**, 1032–1038 (2001).
20. Mangeney, J. *et al.* Continuous wave terahertz generation up to 2 THz by photomixing on ion-irradiated In_{0.53}Ga_{0.47}As at 1.55 μ m wavelengths. *Appl. Phys. Lett.* **91**, 241102 (2007).
21. Samir, R. *et al.* Enhanced terahertz emission from a multilayered low temperature grown GaAs structure. *Appl. Phys. Lett.* **96**, 091101 (2010).
22. Sartorius, B. *et al.* Continuous wave terahertz systems exploiting 1.5 μ m telecom technologies. *Opt. Express* **17**, 15001–15007 (2009).
23. Mikulics, M., Marso, M., Lepsa, M., Grützmacher, D. & Kordo, P. Output Power Improvement in MSM Photomixers by Modified Finger Contacts Configuration. *IEEE Photon. Tech. Lett.* **21**, 146–148 (2009).
24. Pendry, J. B., Martin-Moreno, L. & Garcia-Vidal, F. J. Mimicking surface plasmons with structured surfaces. *Science* **305**, 847–848 (2004).
25. Williams, C. R. *et al.* Highly confined guiding of terahertz surface plasmon polaritons on structured metal surfaces. *Nature Photon.* **2**, 175–179 (2008).
26. Williams, C. R. *et al.* Dual band terahertz waveguiding on a planar metal surface patterned with annular holes. *App. Phys. Lett.* **96**(1), 011101 (2010).
27. Chen, H. T. *et al.* Experimental demonstration of frequency-agile terahertz metamaterials. *Nature Photon.* **2**, 295–298 (2008).
28. Chen, H. T. *et al.* A metamaterial solid-state terahertz phase modulator. *Nature Photon.* **3**, 148–151 (2009).
29. Landy, N. I., Sajuyigbe, S., Mock, J. J., Smith, D. R. & Padilla, W. J. Perfect metamaterial absorber. *Phys. Rev. Lett.* **100**, 207402 (2008).
30. Yu, N. *et al.* Designer spoof surface plasmon structures collimate terahertz laser beams. *Nature Mater.* **9**, 730–735 (2010).
31. Seo, M. A. *et al.* Terahertz field enhancement by a metallic nano slit operating beyond the skin-depth limit. *Nature Photon.* **3**, 152–156 (2009).
32. Berry, C. W., Wang, N., Hashemi, M. R., Unlu, M. & Jarrahi, M. Significant performance enhancement in photoconductive terahertz optoelectronics by incorporating plasmonic contact electrodes. *Nature Comms.* **4**, 1622 (2013).
33. Novotny, L. & Hecht, B. in *Principles of nano-optics* (Cambridge University Press, 2007).
34. Kawano, Y. & Ishibashi, K. An on-chip near-field terahertz probe and detector. *Nature Photon.* **2**, 618–621 (2008).
35. Chen, H.-T. *et al.* Active terahertz metamaterials devices. *Nature* **444**, 597–600 (2006).
36. Large, N., Abb, M., Aizpurua, J. & Muskens, O. L. Photoconductively loaded plasmonic nanoantenna as building block for ultracompact optical switches. *Nano Lett.* **10**, 1741–1746 (2010).
37. Mühlischlegel, P., Eisler, H. J., Martin, O. J., Hecht, B. & Pohl, D. W. Resonant optical antennas. *Science* **308**, 1607–1609 (2005).
38. Tanoto, H. *et al.* Greatly enhanced continuous-wave terahertz emission by nanoelectrodes in a photoconductive photomixer. *Nature Photon.* **6**, 121–126 (2012).

Acknowledgements

H.T. and J.H.T. thank M. Tonouchi for the helpful discussions. This work is financially supported by the Agency for Science, Technology and Research (A*STAR), Singapore, under grant number 082 1410038, 092 1540097 and 092 1540098 and by the Leverhulme Trust in the UK.

Author contributions

J.H.T. conceived the idea and supervised the project. H.T. and Q.Y.W. contributed to the fabrication and characterization of the CW THz photomixer. M.S., Z.N.C., S.A.M. and B.W. contributed to the theory and simulation. H.T. and S.J.C. contributed to the wafer growth. C.C.C., G.Y.S. and A.J.D. contributed to the nano-fabrications. H.T., J.H.T., B.W., M.S. and S.A.M. contributed to the manuscript writing. All the authors discussed the results and reviewed the manuscript.

Additional information

Competing financial interests: The authors declare no competing financial interests.

How to cite this article: Tanoto, H. *et al.* Nano-antenna in a photoconductive photomixer for highly efficient continuous wave terahertz emission. *Sci. Rep.* **3**, 2824; DOI:10.1038/srep02824 (2013).

This work is licensed under a Creative Commons Attribution-NonCommercial-ShareAlike 3.0 Unported license. To view a copy of this license, visit <http://creativecommons.org/licenses/by-nc-sa/3.0>